

Decentralized Control Using Wireless Signal Communication for Multi-Port EV Charger with Multiple Cells

Keita Ohata¹, Hiroki Watanabe², Jun-ichi Itoh¹, Keisuke Kusaka²

¹ Department of Science of Technology Innovation, Nagaoka University of Technology, Nagaoka, Japan

² Department of Electrical, Electronics, and Information Engineering, Nagaoka University of Technology, Nagaoka, Japan

*E-mail: keita_ohata@stn.nagaokaut.ac.jp, hwatanabe@vos.nagaokaut.ac.jp,

itoh@vos.nagaokaut.ac.jp, kusaka@vos.nagaokaut.ac.jp

Abstract— This paper proposes a decentralized control scheme of a multi-cell AC/DC converter for electric vehicle (EV) charger applications. The multi-cell topology effectively achieves high scalability by connecting cells in series and parallel. Generally, the multi-cell topology requires a lot of signal lines between the master control and slave controllers in order to control the power-sharing between the cell converters. Thus, the maintainability of the power converters is restricted with these wires. The proposed control scheme with a wireless communication for the EV charger requires no signal wires between master and slave controllers. The features of the proposed decentralized scheme are; 1) it allows communication delay of several hundred milliseconds, 2) each unit, which consists of three single-phase AC/DC converters, has an independent slave controller. The proposed method is verified by with six units. The power-sharing is demonstrated by the the 7.2-kW prototype. The imbalance rate of the input current is suppressed by 7% or less.

Keywords— battery charger, decentralized control, wireless signal communication, multi-port converter

I. INTRODUCTION

Electric Vehicle (EV) chargers have been important in terms of the growth of EV markets [1]. The EV chargers consist of an isolated AC/DC converter, which has the capability of the Power Factor Correction (PFC) and the DC-DC converter for the output control. An LLC converter and a Dual Active Bridge (DAB) converter have been commonly employed for the isolated DC/DC converters because of their high conversion efficiency by the soft-switching operation [2]-[7]. Recently, the power capacity of the EV batteries and EV chargers has drastically increased in order to extend the cruising distance of EVs. Furthermore, the use scene of EVs and smart micro-grids based on renewable energy sources with energy storage systems are expanding. Thus, the EV charger must widely accept the battery capacity and utilize the energy effectively such as a multi-port converter [8]-[9].

The high-power converter for the EV charger requires a large voltage and current rating for each component of the main circuit. A multi-cell power converter is suitable for the high power converter application because the

circuit configuration is flexibly designed for many system ratings by changing the connection of the cell converters. Especially, the Input-Parallel-Output-Parallel (IPOP) configuration is the typical solution to increase the system current rating for the high-power converters [10]-[12]. However, the multi-cell converter requires many wirings to connect each cell converter. Especially, a lot of signal wiring is necessary in order to control many cell converters by the centralized control. These wiring decreases the system reliability, flexibly and it may become a cause of complicated systems.

The decentralized control for the multi-cell converters has been considered in order to solve those problems [13]. Reference [13] indicates one of the methods, which low-cost communication between the master controller and slave controllers. The system integrates the 5 Mbps optical fiber as the communication line. Thus, It is easy to implement decentralized control. Note that this decentralized control employs the master-slave control in order to regulate all slave controllers which is placed in each cell converter. Hence, the wiring between the master controller and the slave controller is still necessary.

The using wireless communication is suitable to reduce the signal line between master and slave controller. The delay time caused by a wireless communication is several milliseconds to several hundred milliseconds due to queuing and collision avoidance processes if a general-purpose wireless communication module such as Zigbee or Bluetooth is implemented in power converters. Thus, it is not possible to introduce a low-speed control using wireless communication at the inner loop of the voltage or current control into the power converter due to the communication delay of wireless communication.

This paper proposes a decentralized control with the wireless communication, which is suitable for a multi-port EV charger. The originality of this paper is the decentralized control that includes a delay time caused by the wireless communication with the several thousand times larger than the control period. These controls are placed in the outer loop of the fast feedback control, which is each input current control. Therefore, the control allows

a delay of several seconds caused by wireless communication. The validity of the proposed method is demonstrated with a 7.2-kW prototype. From experimented results, the input current imbalance rate is suppressed by 7 % or less.

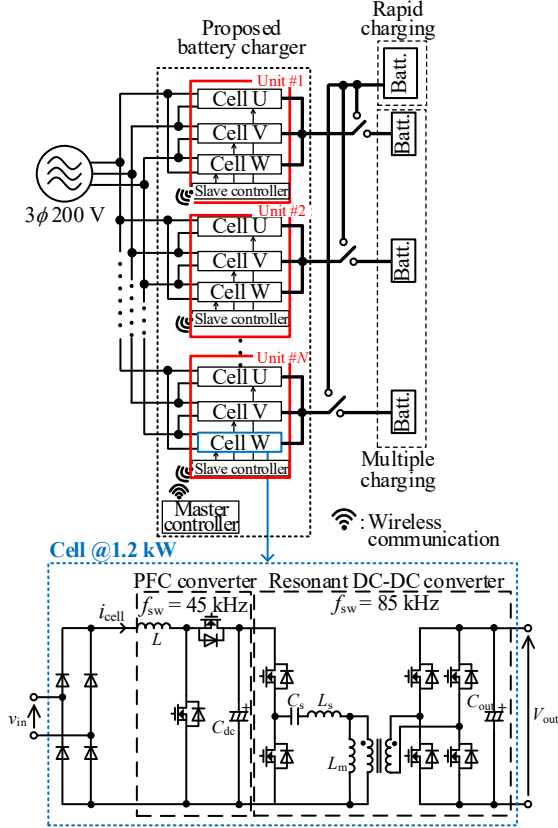


Fig. 1. Multi-port charger system for electric vehicle with multiple cells.

TABLE I
Experimental Conditions.

Quantity	Symbol	value
Input voltage	V_{in}	200 V _{rms}
Rated output power	P	7.2 kW
DC-link capacitance	C_{conv}	1080 μ F ($H = 35$ ms)
Output capacitance	C_{out}	1080 μ F ($H = 35$ ms)
Input inductance	L	3 mH ($\%Z = 2.8\%$)
Switching frequency (PFC)	f_{swPFC}	45 kHz
Switching frequency (Res. DC-DC)	$f_{swDC-DC}$	85 kHz
Angular frequency of PI controller for input current	ω_{ACR}	10000 rad/s
Angular frequency of PI controller for output voltage	ω_{AVR}	50 rad/s

H : Unit capacitance constant of output capacitance based on converter capacity

II. SYSTEM CONFIGURATION AND CIRCUIT TOPOLOGY

Figure 1 shows the system configuration and cell controller. The cell consists of a boost converter to operate PFC and a resonant DC-DC converter. Each phase is connected to three cells in parallel. The resonant DC-DC converter achieves the soft switching with the series resonance between the leakage inductance L_s in the high-frequency transformer and the resonant capacitor C_s connected to the primary side of the transformer. Note that the switching frequency of the DC-DC converter is set to 85 kHz to switch MOS-FETs according to the resonance frequency. Then, the DC-DC converter roles a DC transformer with a constant boost ratio achieving galvanic isolation. The switch on the output side roles the switching between Mode I: Rapid charging and Mode II Multiple charging.

Table I lists the experimental conditions. This paper discusses a case of two units ($N=2$) and the rated power of the cell is designed 1.2 kW. Thus, the rated power of the system is 7.2 kW in this paper.

III. PROPOSED DECENTRALIZED CONTROL SCHEME

Figure 2 (a) shows the control layer diagram of the proposed decentralized control scheme. The master controller manages the system output by communicating with N slave controllers. The master controller transmits the output voltage reference V_{out}^* to slave controllers. Moreover, the averaged input current reference $I_{in_avg}^*$ is transmitted in mode II: rapid charging. Whereas, the slave controllers transmit the input current reference of cell $I_{in_x}^*$ to the master controller.

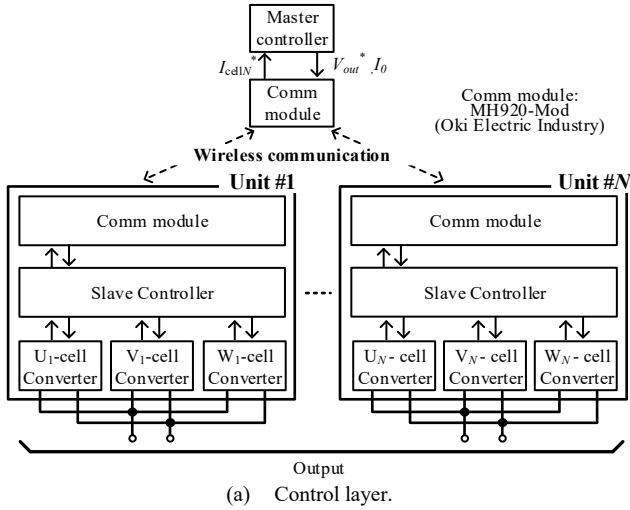
Figure 2 (b) shows the block diagram of the proposed decentralized control. Each input current (I_{in_x}) is controlled by the PI controller to follow the input current reference obtained by the multiplying of the amplitude which is decided by the output voltage controller, and the phase angle that is synchronized with the input voltage. The output voltage is controlled by the PI controller, which is placed on the outer loop of the input current control.

A. Mode I: Multiple charging

The control of mode I: the multiple charging is implemented in a double-loop configuration of the general voltage and current control. In this mode, each slave controller independently controls the input current and the output voltage based on the output voltage reference from the master controller. Then, the output port of each unit is independent of other units. Thus, there is no interference in the output voltage control, and no additional control is required.

B. Mode II: Rapid charging

The output port of the system at mode II is connected in parallel in order to increase the rated capacity of charging to one battery. The slave controllers individually control each output voltage of the cell, thus the control interference between each output voltage controller is caused by the detection error of the output voltage due to the thermal drift characteristics of the detection circuit, and so on. In order to suppress the interference and an



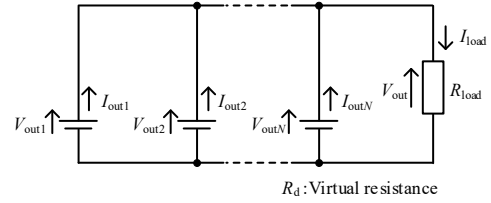
(a) Control layer.
(b) Block diagram.
Fig.2 Proposed decentralized control scheme.

imbalance of the power-sharing between each unit, the output voltage droop control (Section B-1) and the input current balance control (Section B-2) are adopted.

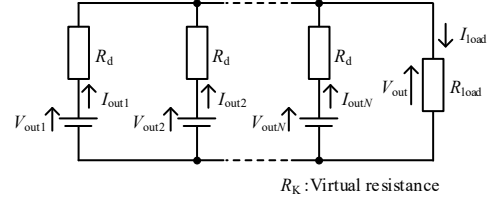
B-1. Output voltage droop control

Figure 3 (a) shows the equivalent circuit of the DC side at mode II. The output of cells is connected in parallel. The output voltage of each cell is controlled by each slave controller. The output voltage is equivalent to a constant voltage source controlled by a feedback controller. Then, the output voltage controller is interference with the mismatched detected output voltage, which is caused by the gain error of the detection or thermal drift of detectors. In order to adapt to this problem, the output voltage droop control is adopted as the non-interference control between the parallel-connected converters.

Figure 3(b) shows the equivalent circuit of the DC side, which is adapted to output voltage droop control. The droop control acts as the series-connected resistance to constant voltage source controlled by each slave controller.



(a) without output voltage control.



(b) with output voltage control.

Fig.3 Equivalent circuit of DC side at mode II: rapid charging.

Thus, the control suppresses the interference between each output voltage control.

B-2. Input current balance control

The role of the input current balance control is the prevention of the current deviation between the input current of unit converters. For example, the detected output voltage of unit #1 has positive error, the output voltage of unit #1 is controlled to lower voltage than another unit. Thus, the input current of unit #1 is controlled to small than another unit. It indicates the imbalance of power sharing between unit.

The control compensates the output voltage reference using a PI controller based on the difference which is the input current reference I_{in_x} and the averaged input current reference I_{in_avg} .

B-3. Wireless signal communication between master and slave controllers

The master controller transmits the output voltage reference V_{out}^* and the averaged input current reference $I_{in_avg}^*$ to slave controllers. Moreover, the master controller receives the input current reference $I_{in_x}^*$ from the slave controllers at mode II. The averaged input current reference $I_{in_avg}^*$ is given by

$$I_{in_avg}^* = \frac{1}{N} \sum_{x=1}^N (I_{in_x}^*) \quad (1)$$

The slave controller corrects the output voltage reference based on the above wireless communication by the output voltage droop control. the input current balance control in order to achieve the power-sharing and non-interference.

IV. CHARACTERISTIC OF PROPOSED DECENTRALIZED CONTROL SCHEME

A. Communication period between master and slave controller T_{comm}

The minimum communication period between the master and slave controller $T_{comm(min)}$ is limited by the communication delay time of the communication module. Moreover, the maximum communication period $T_{comm(max)}$ is limited by the allowable settling time to compensate the

imbalance of the input current. The settling time becomes longer as the communication delay time increases. Well-known the wireless communication (e.g., Zigbee, Bluetooth) has from several milliseconds to several hundred of milliseconds delay as a communication delay due to queuing processing, and so on. Thus, the settling time may reach up from several hundred milliseconds to several seconds when these wireless module is employed. However, the long settling time of the input current is not a significant problem from the point of view of a rapid charger for EVs because of the relatively stable load.

B. Virtual droop resistance R_d

This chapter discusses the effect of increasing or decreasing the virtual droop resistance on the prevention of the control interference between the output voltage controllers. The non-interference is easily achieved when the virtual droop resistance R_d which is in series with each voltage source increases, whereas the error between the output voltage and the output voltage reference increases. Thus, the droop resistance should be as small as possible.

The condition for the prevention of the interference in each voltage control system is given by

$$V_{out_x}^* > V_{out} \quad (2)$$

where $V_{out_x}^*$ is output voltage reference of each slave controller, x is unit number ($x = 1 \sim N$), V_{out} is output voltage. That is when the output voltage reference value $V_{out_x}^*$ of each cell unit exceeds the output voltage V_{out} , non-interference of the output voltage control system is achieved.

In this paper, an acceptable output voltage error of up to $\pm 5\%$ is specified, and the droop resistance R_d is set to 5% of rated impedance to satisfy this specification.

The input current balance control is placed on the outer of the PI controller of the output voltage. Hence, the bandwidth of the input current balance control is designed with slower than the output voltage PI controller. The balance control uses the averaged input current reference I_{in-avg}^* obtained by low-speed wireless communication, it is necessary to design the system with the communication cycle T_{comm} in mind. Thus, by the integral time constant T_i is set to 1.5 second and the proportional gain K_p is set to 1.0 using the ultimate sensitivity method.

V. EXPERIMENTAL RESULTS

Table II lists the specification of the wireless communication module. A wireless communication module MH920 (Oki Electric Industry) is employed. The data length of the output voltage reference and the averaged input current reference is set to 2 bytes. Note that the header and footer packets are added to the communication data according to the protocol of the wireless communication module. Figure 4 (a) shows the cell converters. The charger system consists of six cells. Figure 4 (b) shows the master/slave controller and wireless module. The MCU (Microcontroller Unit) is TMS320F28379D (Texas Instruments). The MCU communicates the wireless module using UART (Universal Asynchronous Receiver/Transmitter) with 115,200 bps. In this case, due to the constraints of the control program and wireless module, The communication period is set to 1.0 sec to prevent hang-up due to communication congestion.

A. Communication delay caused by wireless module

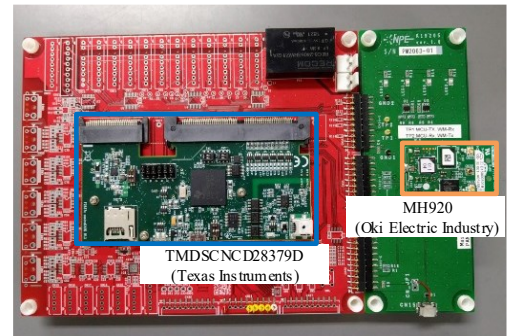
Figure 5 shows the communication waveform between master and slave. The master controller transmits output voltage reference and input current reference to slave controllers #1 through #N in sequence. Each output voltage command value is transmitted with a time difference of milliseconds and updated every seconds. Systems that include Zig-bee, Bluetooth, and other general-purpose wireless communications generally have communication delays of several tens of milliseconds or

TABLE II
SPECIFICATION OF WIRELESS COMMUNICATION MODULE

Manufacture	Oki Electric Industry
Frequency band	920 MHz
Product name	Coordinator: MH920-Mod<1><0S> Router: MH920-Mod<1><0W>
Module size	23.9 mm × 40.9 mm × 5 mm
Maximum number of connection	100



(a) Cell converter.



(b) Master/slave controller and wireless module.

Fig. 4 Photograph of electric vehicle charger system.

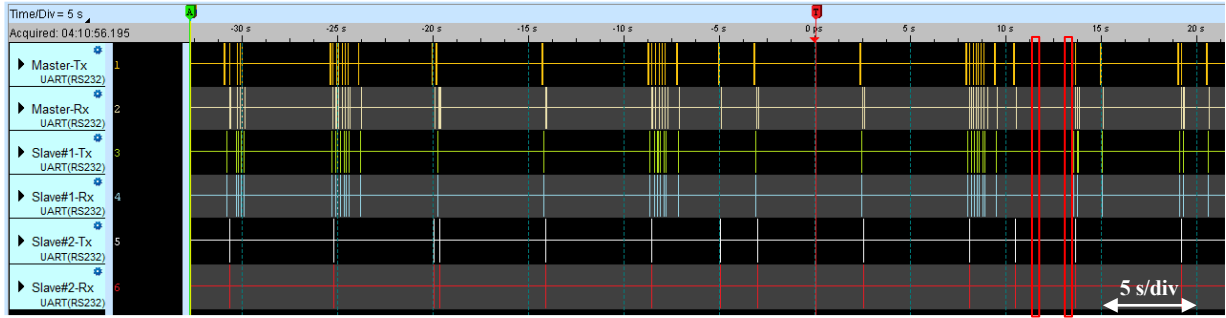
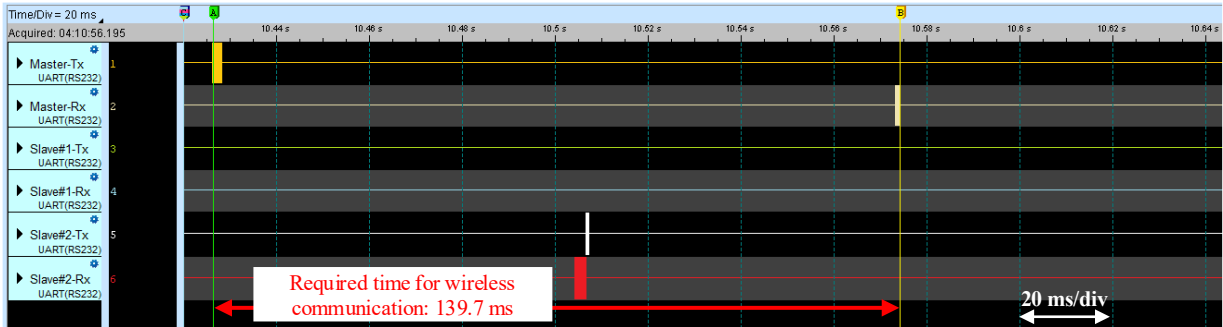
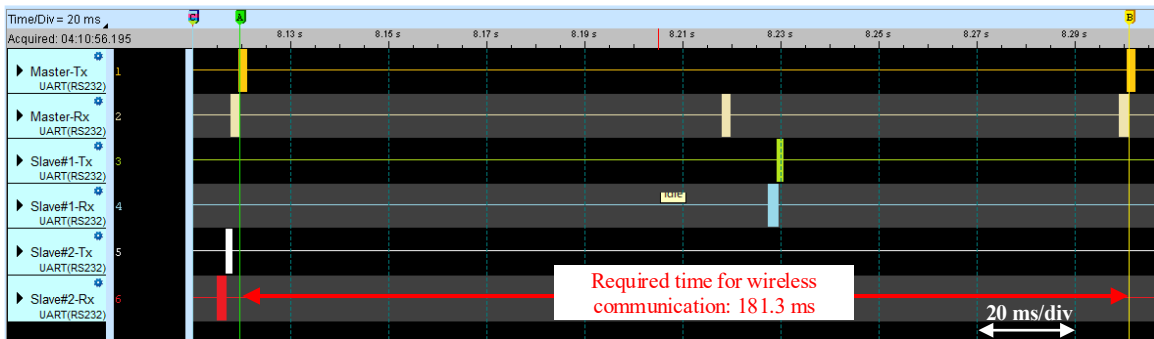


Fig. 5 (b) Fig. 5 (c)

(a) Outline.



(b) Extended Fig. 5(a): Transmission of the data in the master controller to the slave controller #2.



(c) Extended Fig. 5(a): Reception of the data in the slave controller #1 to the master controller.

Fig. 5 Waveform of wireless communication in the proposed method.

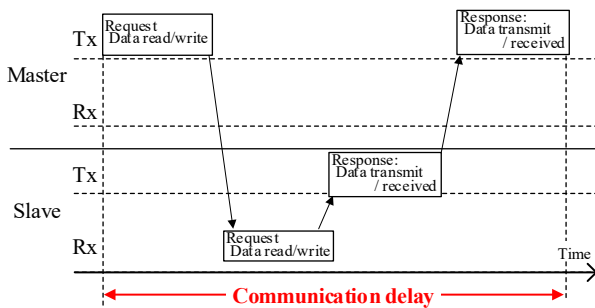


Fig.6 Procedure of wireless communication. the communication delay caused by wireless communication is defined as shown the figure.

more due to queuing processing, congestion processing, etc. Moreover, the communication delay is variable as shown in Fig.5(b), (c), and Fig.7.

Figures 5(b) shows a measured communication delay time according to the definition in Fig. 6, when the transmission of the data in the master controller MCU to the slave controller #2 MCU is processing. The data

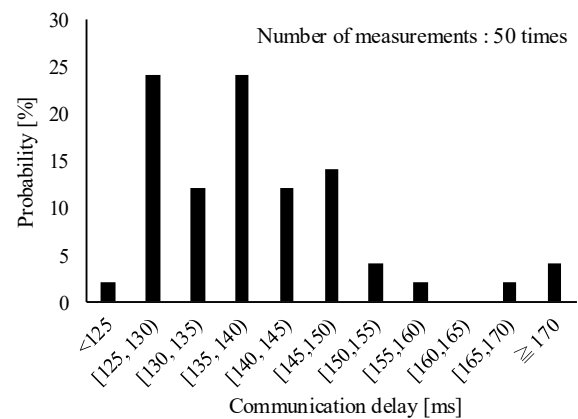


Fig.7 Distribution of wireless communication delay in the communicating sequence, which is reception of the data in slave controllers to the master controller.

transmit command arrives at the Rx (receive) of Slave #2 MCU after 10 milliseconds which the signal is output from

the Tx (transmit) of the master MCU. The requested data is sent back to the master controller in about 60 milliseconds. Thus, the sequence of the transmission of the data in the master controller to slave is required at 139.7 milliseconds in this case.

Figure 5(c) shows a measured communication delay time according, when the reception of the data in the slave controller #1 to the master controller is processing. The data transmit command arrives at the Rx (receive) of Slave #2 MCU after 10 milliseconds which the signal is output from the Tx (transmit) of the master MCU. The requested data is sent back to the master controller in about 70 milliseconds. Thus, the sequence of the data request command from slave to master takes 181.3 milliseconds.

Figure 7 shows the histogram of the delay time caused by wireless communication obtained by 50 measurements in the experimental condition. The mode value of the histogram is from 125 milliseconds to 130 milliseconds and 135 milliseconds to 140 milliseconds. Moreover, the minimum/maximum of the delay is 122/181 milliseconds under the experimental conditions. Note that, this histogram is only example, as it varies depending on the wireless communication standard, the congestion of the transmission line, the kind of wireless module. Thus, a design of the controller for power converters using wireless communication must be keep in mind that the variation in communication delay time is large.

B. Mode I: Multiple charging

Figure 8 shows the input current and output voltage waveforms at a steady state. At this time, the two chargers are controlled to output voltage independently, and the master controller transmits only output voltage reference 350 V. The output voltage follows the reference value of 350V. The output power is uniformly supplied from each cell according to the load to each unit.

C. Mode II: Rapid charging

Figure 9 shows the input current and output voltage waveforms at 4.3 kW (0.6p.u.). The detected output voltage of cell #1 adds +2% detected error. In contrast to mode I, mode II adds the output voltage droop control because the output ends are connected in parallel. In addition, input current balance control is added to prevent power imbalance between units due to output voltage detection errors. The input current amplitude of units #1 equals with #2, despite the error in the detected voltage of unit #1. The imbalance rate of the input current ε_{in} is defined by (3).

$$\varepsilon_{in}[\%] = \left| \max \left\{ \frac{I_{cell_x} - I_{in-avg}}{I_{in-avg}} \right\} \right| \times 100 \quad (x=1 \sim N) \quad (3)$$

where I_{cell_x} is each input current, I_{in-avg} is averaged input current. The imbalance ratio is 7% and the current deviation between cells was kept below 1 A, and each input current of cell is balanced.

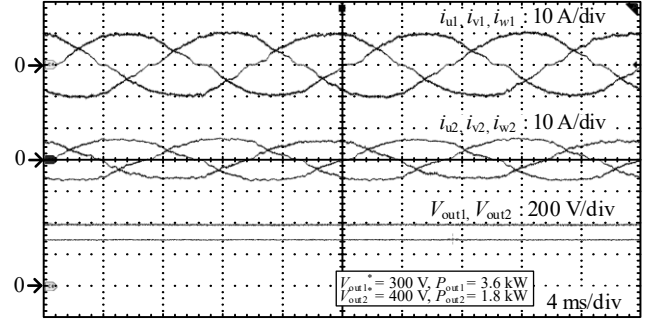
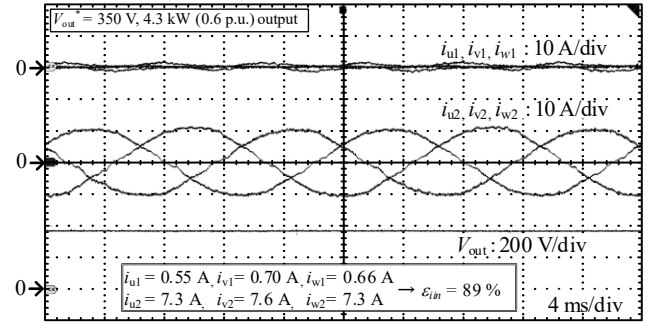
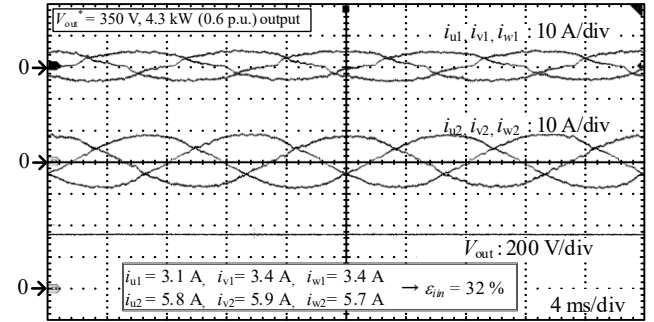


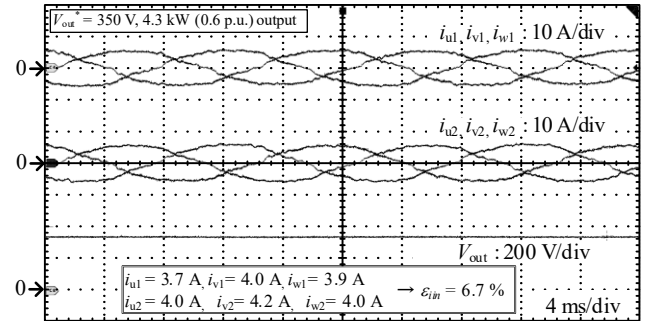
Fig. 8 Input current and output voltage at steady state in mode I: multiple charging.



(a) Without input current balance and without output voltage droop control.



(b) Without input current balance and with output voltage droop control.



(c) With input current balance and with output voltage droop control.

Fig. 9 Input current and output voltage at steady state in mode II. The detected output voltage of cell #1 adds +2% detected error.

Figure 9 (a) shows the input current and the output voltage without proposed input current balance control and without output voltage droop control. The input currents i_{u1} , i_{v1} , and i_{w1} of unit #1 are almost zero, and the imbalance of the input current occurs.

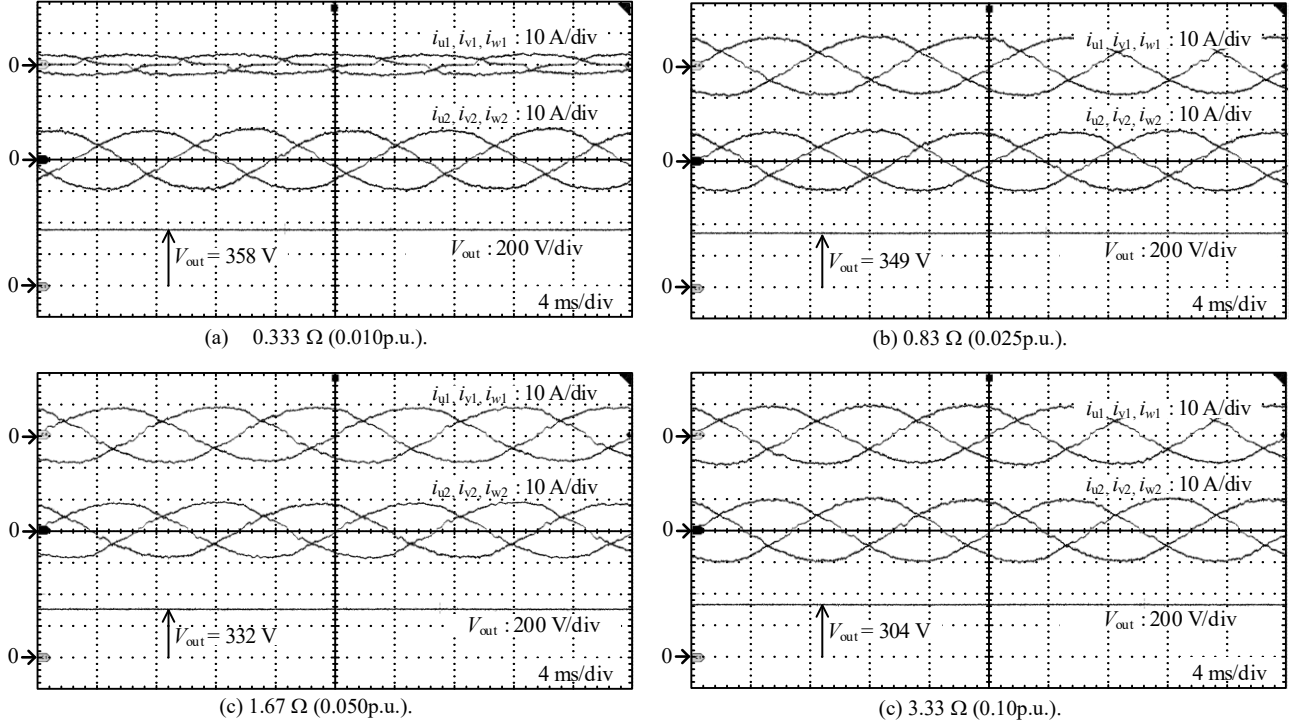


Fig.10 Input current and output voltage when droop resistance is changed from 0.01p.u. to 0.1p.u. $V_{out}^* = 350$ V.

Figure 9 (b) shows the input current and the output voltage without proposed input current balance control and with output voltage droop control. The input currents are averaged by the droop control, the input currents i_{u1} , i_{v1} , and i_{w1} of unit #1 are controlled smaller than the input currents of unit #2 i_{u2} , i_{v2} , and i_{w2} due to the positive error in the output voltage detection value of unit #1. Thus the input current is imbalanced. The control results in a decrease from $\varepsilon_{in} = 89\%$ to $\varepsilon_{in} = 32\%$.

Figure 9 (c) shows the the input current and the output voltage waveform with proposed input current balance control and output voltage droop control. The imbalance of input current caused by output voltage error is compensated by input current balance control. The control results in a decrease from $\varepsilon_{in} = 32\%$ to $\varepsilon_{in} = 6.7\%$.

D. Characteristics of proposed decentralized control.

Figure 10 shows the input current and output voltage waveform when droop resistance R_d is changed from 0.01p.u. to 0.1p.u. The output voltage reference is set to 350 V. the output voltage error increases with the increase of the droop resistance increases. The minimum droop resistance is determined by the allowable output voltage error. Thus, the design of tolerance for the error of detected output voltage is better which is lower.

Figure 11 and Figure 12 shows the input current and output voltage waveform when T_{comm} is changed. In Fig.11, T_{comm} is set to 5 seconds, and in Fig.12, T_{comm} is set to 10 seconds. The output voltage reference is set to 350 V. The transient response is not related when the communication delay time is varied because input current balance control, which uses wireless communication parameters, is used only in order to compensate for the imbalance of input current caused by output voltage errors, whereas the

transient load variations are controlled only by the output voltage droop control, which does not use wireless communication. Thus, the balanced state is continued which has an output voltage detection error.

VI. CONCLUSION

This paper proposed the decentralized control scheme, which is included low-speed communication from 100 milliseconds to one seconds using wireless communication. The proposed scheme is characterized by the output voltage droop control and the input current balance control, which adapt wireless signal communication. The proposed scheme requires no signal lines between the master controller and slave controllers. These characterized controls are placed in the outer loop of the fast feedback control of input current and voltage controller. Therefore, the control allows several hundred of milliseconds delay of wireless communication. Moreover, the signal communication The proposed scheme is verified by experiments with the 7.2-kW prototype. From experimental results, the imbalance rate of input current ε_{in} is suppressed by 7% or less with low communication period.

In the future work, the response evaluation by communication delay time and design method of droop gain is going to be studied in more detail.

REFERENCES

- [1] International Energy Agency, "Global EV Outlook 2021", 2021
- [2] Y. Yan, H. Bai, C. Yang and W. Wang, "Securing Full-load-range Zero Voltage Switching for A Dual Active Bridge Based Electric Vehicle Charger," 2020 IEEE Applied Power Electronics Conference and Exposition (APEC), pp. 2067-2072, 2020.
- [3] Yuki Kinoshita, Hitoshi Haga, "Wide-Range Voltage Gain and High-Efficiency of Isolated LLC Converter using Six-Switch and

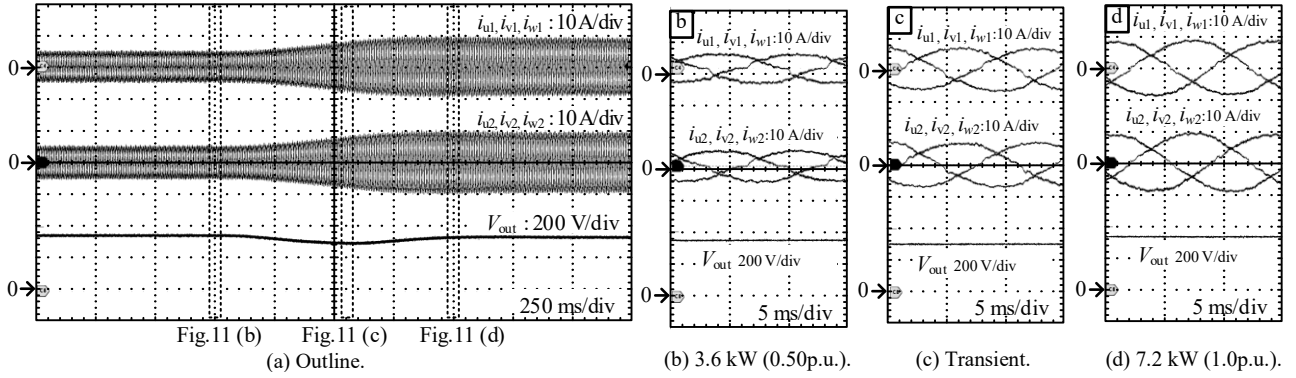


Fig.11 Input current and output voltage when load is changed from 3.6 kW (0.50p.u.) to 7.2 kW (1.0p.u.). $V_{out}^* = 350$ V, $T_{comm} = 5$ sec.

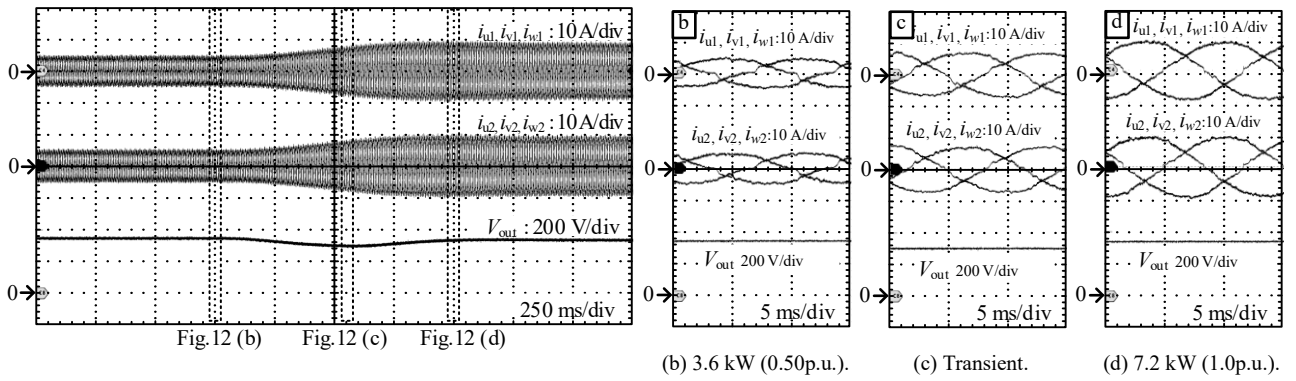


Fig.12 Input current and output voltage when load is changed from 3.6 kW (0.50p.u.) to 7.2 kW (1.0p.u.). $V_{out}^* = 350$ V, $T_{comm} = 10$ sec.

- Two Asymmetric Transformers”, IEEJ J. Industry Applications, vol.9, no.6, pp.703-712, 2020.
- [4] Hwa-Pyeong Park, Yesung Kang, Seokhyeong Kang, Jee-Hoon Jung, “FPGA Controller Design for High-Frequency LLC Resonant Converters”, IEEJ J. Industry Applications, vol.9, no.5, pp.523-529, 2020.
- [5] Sandeep Kumar Chowdhury, Hiroyasu Kobayashi, Keiichiro Kondo, “Design Optimization of Power Electronic Transformers in Traction Applications”, IEEJ J. Industry Applications, vol.9, no.6, pp.674-684, 2020.
- [6] Yutaro Tashiro, Hitoshi Haga, Improvement of Light-Load Efficiency by using a Six-Arm Converter with Series-Parallel Switching, IEEJ J. of Industry Applications, vol.10 no.2, pp.273-281, 2021.
- [7] H. Bai and C. Mi, “Eliminate Reactive Power and Increase System Efficiency of Isolated Bidirectional Dual-Active-Bridge DC–DC Converters Using Novel Dual-Phase-Shift Control”, IEEE Transactions on Power Electronics, vol. 23, no. 6, pp. 2905-2914, 2008.
- [8] S. A. Khan, M. R. Islam, Y. Guo and J. Zhu, “A New Isolated Multi-Port Converter With Multi-Directional Power Flow Capabilities for Smart Electric Vehicle Charging Stations”, IEEE Transactions on Applied Superconductivity, vol. 29, no. 2, pp. 1-4, 2019.
- [9] K. Suresh et al., “A Multifunctional Non-Isolated Dual Input-Dual Output Converter for Electric Vehicle Applications”, IEEE Access, vol. 9, pp. 64445-64460, 2021.
- [10] Y. Xia, M. Yu, Y. Zhang, Z. Lv and W. Wei, “Decentralized Suppression Strategy of Circulating Currents Among IPOP Single-Phase DC/AC Converters,” in IEEE Journal of Emerging and Selected Topics in Power Electronics, vol. 8, no. 2, pp. 1571-1583, 2020.
- [11] J. Shi, L. Zhou and X. He, “Common-Duty-Ratio Control of Input-Parallel Output-Parallel (IPOP) Connected DC–DC Converter Modules With Automatic Sharing of Currents,” in IEEE Transactions on Power Electronics, vol. 27, no. 7, pp. 3277-3291, 2012.
- [12] Y. Xia, M. Yu, Y. Zhang, Z. Lv and W. Wei, “Decentralized Suppression Strategy of Circulating Currents Among IPOP Single-Phase DC/AC Converters,” in IEEE Journal of Emerging and Selected Topics in Power Electronics, vol. 8, no. 2, pp. 1571-1583, 2020.
- [13] J. Nie, L. Yuan, Q. Gu, J. Sun and Z. Zhao, “A Coordinate and Distributed Control Scheme for Multilevel and Multi-Stage Medium Voltage Solid State Transformer,” 2018 International Power Electronics Conference (IPEC-Niigata 2018 -ECCE Asia), pp. 2963-2968, 2018.